NACA RM A51LO3a

NACA

RESEARCH MEMORANDUM

SOME EFFECTS OF SIDE-WALL MODIFICATIONS ON THE DRAG AND PRESSURE RECOVERY OF AN NACA SUBMERGED INLET AT TRANSONIC SPEEDS

By Robert A. Taylor

Ames Aeronautical Laboratory
Moffett Field, Calif.

NATIONAL ADVISORY COMMITTEE
FOR AERONAUTICS

WASHINGTON

February 15, 1952

NATIONAL ADVISORY COMMITTEE FOR AERONAUTICS

RESEARCH MEMORANDUM

SOME EFFECTS OF SIDE-WALL MODIFICATIONS ON THE DRAG AND PRESSURE RECOVERY OF AN NACA SUBMERGED INLET AT TRANSONIC SPEEDS

By Robert A. Taylor

SUMMARY

Comparative drag and pressure recovery were measured for an NACA submerged inlet and two side-wall modifications thereof. A common afterbody and diffuser were used for all tests. The investigation was conducted over a Mach number range from 0.80 to 1.11 by the use of the transonic bump in the Ames 16-foot high-speed wind tunnel. Ram-recovery ratio was measured for mass-flow ratios from 0 to 0.93.

The two modified inlets were generally superior to the standard inlet from the standpoint of pressure recovery, at the highest test mass-flow ratios, about 0.88.

For the highest test mass-flow ratios, no significant changes in drag were produced by the modifications for Mach numbers below 1.0, but small increases in drag over that of the NACA submerged inlet prevailed at supersonic Mach numbers for the higher angles of attack.

INTRODUCTION

Ram-recovery contours from previous investigations (references 1 and 2) indicated that vortices formed above the diverging ramp walls, entrained low-energy body boundary-layer air, and, upon entering the inlet, resulted in reduced pressure recovery. It is believed that the vortices are beneficial for thinning the boundary layer along the ramp floor, but upon entering the air-induction system they manifest themselves in the form of total-pressure losses. It was reasoned that increasing the angle between the body contour and ramp wall would reduce the strength of the ramp-wall vortices and displace them outwardly. It was anticipated that the vortices, though weakened, would still be of

sufficient strength to aid in sweeping the submerged inlet boundary-layer air out and over the ramp walls. Also it was reasoned that the displacement of the vortices would result in a smaller part of the vortices being ingested by the induction system. (See fig. 1.)

NOTATION

A	duct entrance area 0.40 inch downstream of lip leading edge, square feet
H	total pressure, pounds per square foot
M	Mach number
m	mass flow (ρAV), slugs per second
p	static pressure, pounds per square foot
q	dynamic pressure ($\frac{1}{2}\rho V^2$), pounds per square foot
S	cross-sectional area of half-body, square feet
V	velocity outside the boundary layer, feet per second
C_D	total drag coefficient of the inlet and body combination, including internal drag $\left(\frac{\text{drag}}{q_o 2S}\right)$
$\frac{H_1 - p_o}{H_o - p_o}$	ram-recovery ratio at the inlet rake
$\frac{m_1}{m_o}$	ratio of the mass flow through the inlet to the mass flow in the free stream through an area equal to the inlet area $\left(\frac{\rho_1 A V_1}{\rho_o A V_o}\right)$
α	angle of attack of the side-inlet model, degrees
ρ	mass density, slugs per cubic foot

Subscripts

o	free stream
1	inlet rake station

APPARATUS

A description and photograph of the Ames 16-foot high-speed wind-tunnel bump were presented in reference 2.

Three inlet variations were compared in this investigation: an NACA submerged inlet (the same submerged inlet used in reference 1), and two modifications of this inlet. The same afterbody and diffuser were used with each of the three variations. Figure 2 shows the three bodies with side inlets mounted on the transonic bump. Details and dimensions of the three inlets and the accompanying afterbody are given in figures 3 and 4.

The NACA submerged inlet was modified by increasing the angle between the ramp floor and walls. (See fig. 4.) Since these ramp walls were warped, no one element angle indicated the angle of wall slope. For this reason the angle of wall slope used to define the inlets was taken as the angle between the ramp floor and ramp wall at station 15 which is located at the lip leading edge of the duct entrance. The three inlets will hereafter be referred to as the NACA submerged inlet, the 134° inlet, and the 146° inlet. Each wall element for the 134° inlet was generated by passing a line from the model center line tangent to the fillets joining the ramp floor and walls. The wall elements for the 146° inlet were similarly generated except that the center line was transposed 1/2 inch outboard and parallel to its original position. The typical sections shown in figure 4 represent this pictorially.

Internal diffusion of the air began 0.4 inch downstream from the lip leading edge and continued to within 1 inch of the exit. The entrance area was 2 square inches measured at a distance of 0.4 inch from the lip leading edge. The maximum exit area was 3.14 square inches and provisions were made to vary the exit area by the use of various angular constrictions. All models were mounted 0.75 inch from the bump surface to place the model outside the influence of the bump boundary layer. Between the model and the bump surface an underbody was mounted; the underbody had the same profile as the model adjacent to the bump and was fastened to the bump.

The inlet rake was mounted in the diffuser with the tube openings 2.75 inches downstream from the lip leading edge, the net area at this station being equal to the entrance area. The inlet rake was constructed so that each of 19 total-pressure tubes was located in the center of an equal area; 14 static-pressure tubes were interspaced among the total-pressure tubes. Mass-flow ratio and ram-recovery ratio were computed from the inlet-rake data. The total drag of the model was measured by a strain-gage balance located within the bump.

TESTS

The four test angles of attack were 0°, 3°, 6°, and 9°. Annular exit constrictions were used to vary the exit area, thereby varying the mass-flow ratio. Ram-recovery and mass-flow data for the NACA submerged inlet were measured for exit-area ratios of 1.00, 0.75, 0.25, and 0 at 0° and 6° angle of attack. For 3° and 9° angle of attack, mass-flow and ram-recovery data were measured with an exit-area ratio of 1.00. Ram-recovery and mass-flow data were measured at 0°, 3°, 6°, and 9° with exit-area ratios of 1.00, 0.50, 0.25, and 0 for the two modified inlets. Exit-area ratio is defined as the ratio of a given exit area to the maximum exit area. Drag was measured for the four angles of attack with the exit full open throughout the Mach number range.

REDUCTION OF DATA

The ram-recovery ratio at the inlet rake was calculated by the method described in reference 3 wherein the logarithm of total pressure at each of the 19 tubes in the rake was weighted by the mass flow through the area assigned to that tube. The mass-flow ratio was computed as the summation of the mass flows through the 19 assigned areas. Further discussion of this method of computation may be found in reference 1, page 9. Ram-recovery and mass-flow ratios presented in the present report generally could be determined within increments of ± 0.01.

Drag coefficients shown include internal drag but, since the same afterbody and diffuser were used, the internal drag remains relatively constant at any given mass-flow ratio for the inlet configurations tested. The accuracy of the experimental drag-coefficient data was estimated to be ± 0.005.

The Mach number was determined by the method of reference 2. Mach number measurements were consistent within ± 0.01. The actual Mach number, however, was difficult to determine because of the streamwise Mach number gradient on the bump. (See reference 2.) Measurement of the angle of attack was accurate to within approximately 0.1°.

RESULTS

The results in this report are presented as follows:

1. Variations of ram-recovery ratios and mass-flow ratios with Mach number, for constant angles of attack (figs. 5, 6, 7)

2. Cross plots of figures 5, 6, and 7 depicting ram-recovery ratio as a function of mass-flow ratio (fig. 8)

3. Comparative variation of increment of ram-recovery ratio as a function of Mach number (fig. 9)

4. Contours of ram-recovery ratio (fig. 10)

5. Variation of drag coefficient with Mach number (fig. 11)

DISCUSSION

Ram-Recovery Ratio

Effect of mass-flow ratio.- Curves of ram-recovery ratio as a function of mass-flow ratio for the three inlets (fig. 8) indicate that the modified versions generally yielded higher ram-recovery ratios than the NACA submerged inlet at the highest test mass-flow ratio, about 0.88. At about 0.4 mass-flow ratio the NACA submerged inlet yielded pressure recoveries about the same or greater than those of the modified inlets.

The improvement in ram recovery resulting from the modifications at the highest test mass-flow ratios is believed to be produced by the outward displacement of the vortices generated by the ramp walls, and the escape of accumulated ramp-wall boundary layer which passed outside of the entrance. An inspection of figure 10(a) shows the presence of what is believed to be accumulated boundary layer in the upper and lower regions adjacent to the ramp side. These phenomena are not apparent in figures 10(b) and (c) and it was therefore assumed that the modifications performed their design function. As for the displaced vortices, a comparison of the three contours 10(a), (b), and (c) shows that a decrease in the size or an outward shift of the low-energy areas accompanies the modification of the inlets. The afore-mentioned areas were located at the upper and lower lip side of the inlet.

Effects of Mach number and angle of attack.- Figure 9 shows the ram-recovery-ratio increments for the two modified inlets as compared to the

NACA submerged inlet at the highest test mass-flow ratios which are the more significant for practical flight requirements. This comparison indicated that for all test angles of attack and Mach numbers the two modified inlets generally yielded equal or superior pressure recovery.

Drag

The total-body-drag coefficients for the three inlet configurations are presented in figure 11. For these comparisons the exit was full open.

At 0° angle of attack the three inlets had essentially the same drag and for the other angles of attack there was no increase in drag for the modified inlets over that of the NACA submerged inlet until after a Mach number of 1.0 was reached. At supersonic Mach numbers the drag of the modified inlets was slightly greater than that of the NACA submerged inlet at the higher angles of attack.

There is some doubt as to the validity of the method of determining drag for this investigation, and for that reason only comparative values of the drag data are considered.

CONCLUSIONS

1. For free-stream Mach numbers below 1.0, a mass-flow ratio of approximately 0.88, and angles of attack between 0° and 9°, the ram-recovery ratio of the modified inlets was generally increased over that of the NACA submerged inlet.

2. For the mass-flow ratios of about 0.88, no significant changes in drag were produced by the modifications for Mach numbers below 1.0, but small increases in drag accompanied the gains in ram-recovery ratio resulting from the modifications at supersonic Mach numbers for the higher angles of attack.

Ames Aeronautical Laboratory,
National Advisory Committee for Aeronautics,
Moffett Field, Calif.

REFERENCES

1. Frank, Joseph L., and Taylor, Robert A.: Comparison of Drag, Pressure Recovery, and Surface Pressure of a Scoop-Type Inlet and an NACA Submerged Inlet at Transonic Speeds. NACA RM A51H20a, 1951.

2. Axelson, John A., and Taylor, Robert A.: Preliminary Investigation of the Transonic Characteristics of an NACA Submerged Inlet. NACA RM A50C13, 1950.

3. Hall, Charles F., and Barclay, F. Dorn: An Experimental Investigation of NACA Submerged Inlets at High Subsonic Speeds. I - Inlets Forward of the Wing Leading Edge. NACA RM A8B16, 1948.

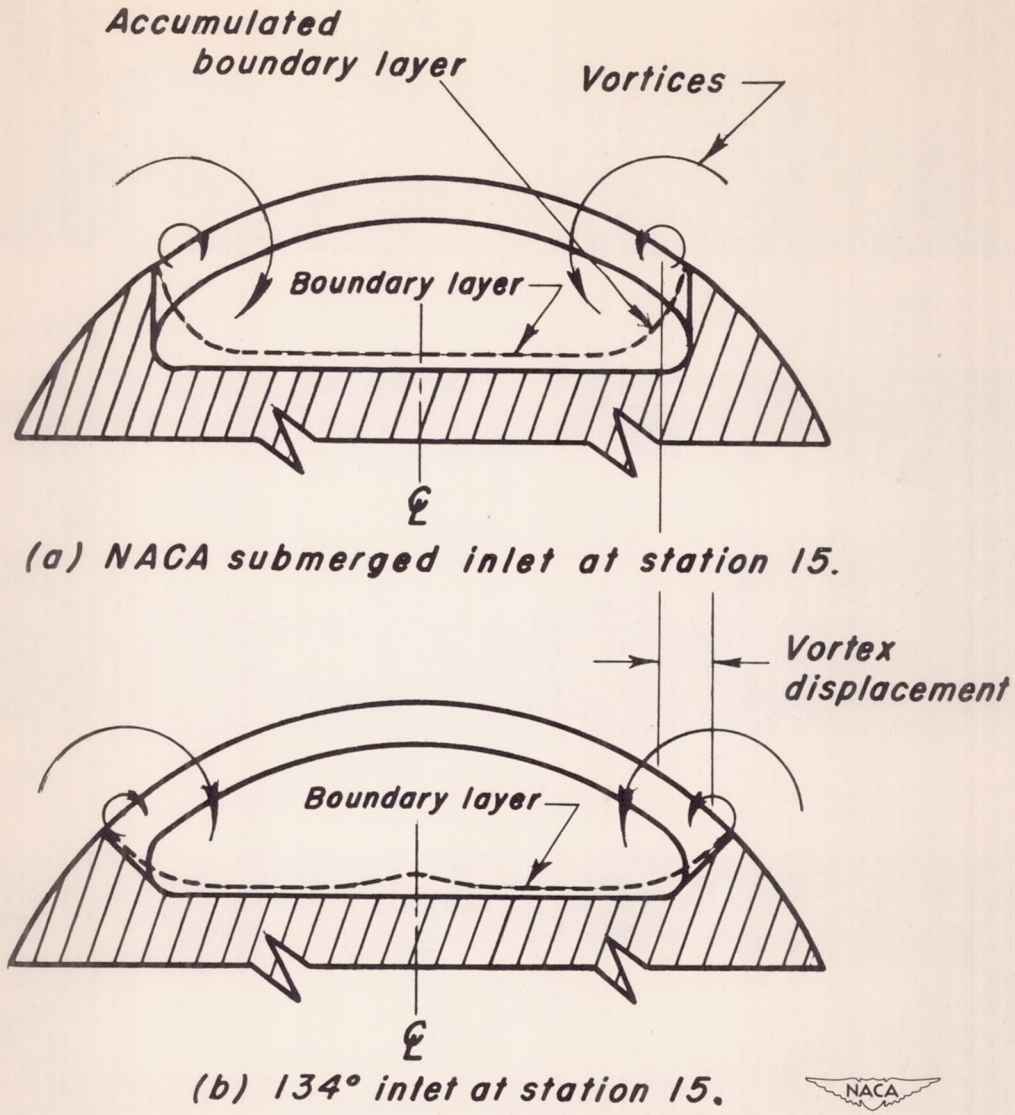

Figure 1.—Sketch of vortex formation and boundary layer on the ramp walls and floor of the NACA submerged inlet and the 134° inlet.

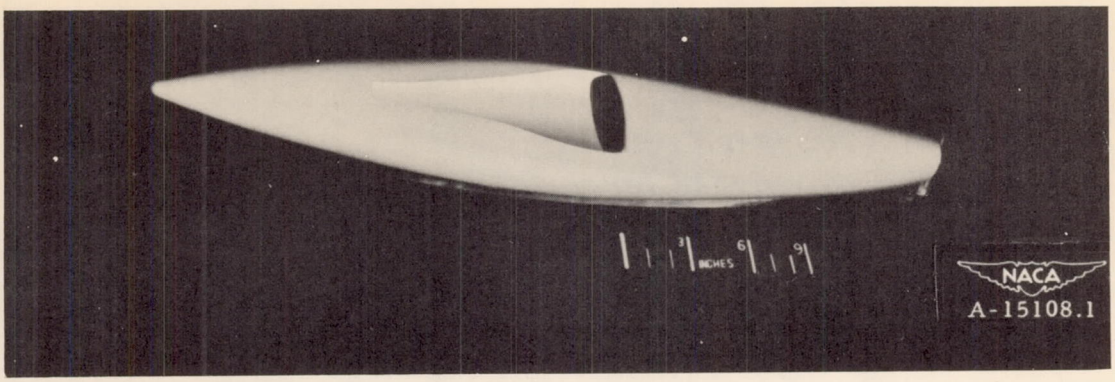

(a) Body with NACA submerged inlet.

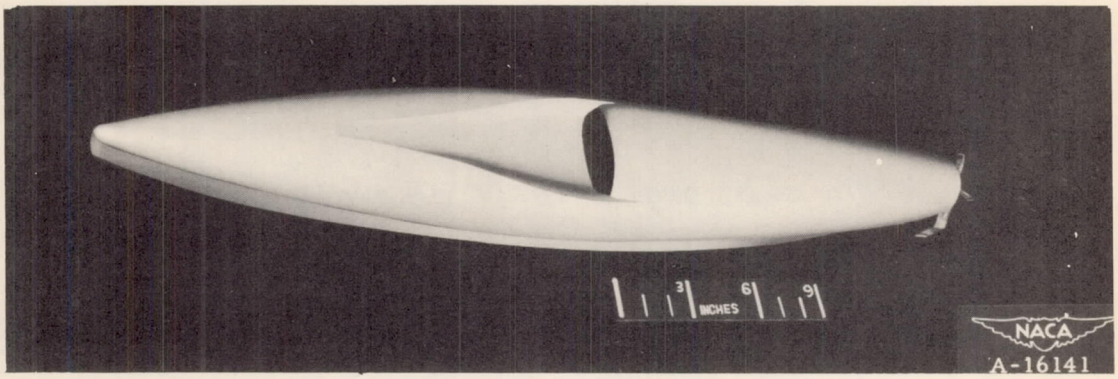

(b) Body with the 134° inlet.

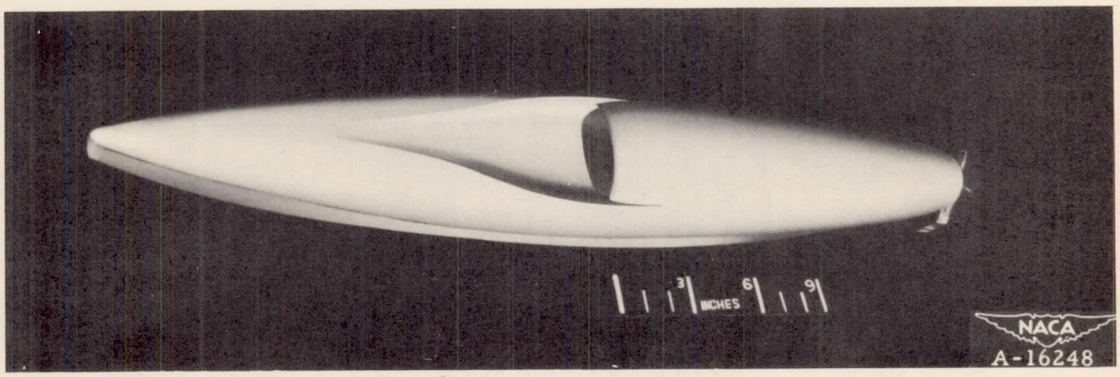

(c) Body with the 146° inlet.

Figure 2.– Model of NACA submerged inlet and two modifications mounted on the transonic bump in the Ames 16–foot high–speed wind tunnel.

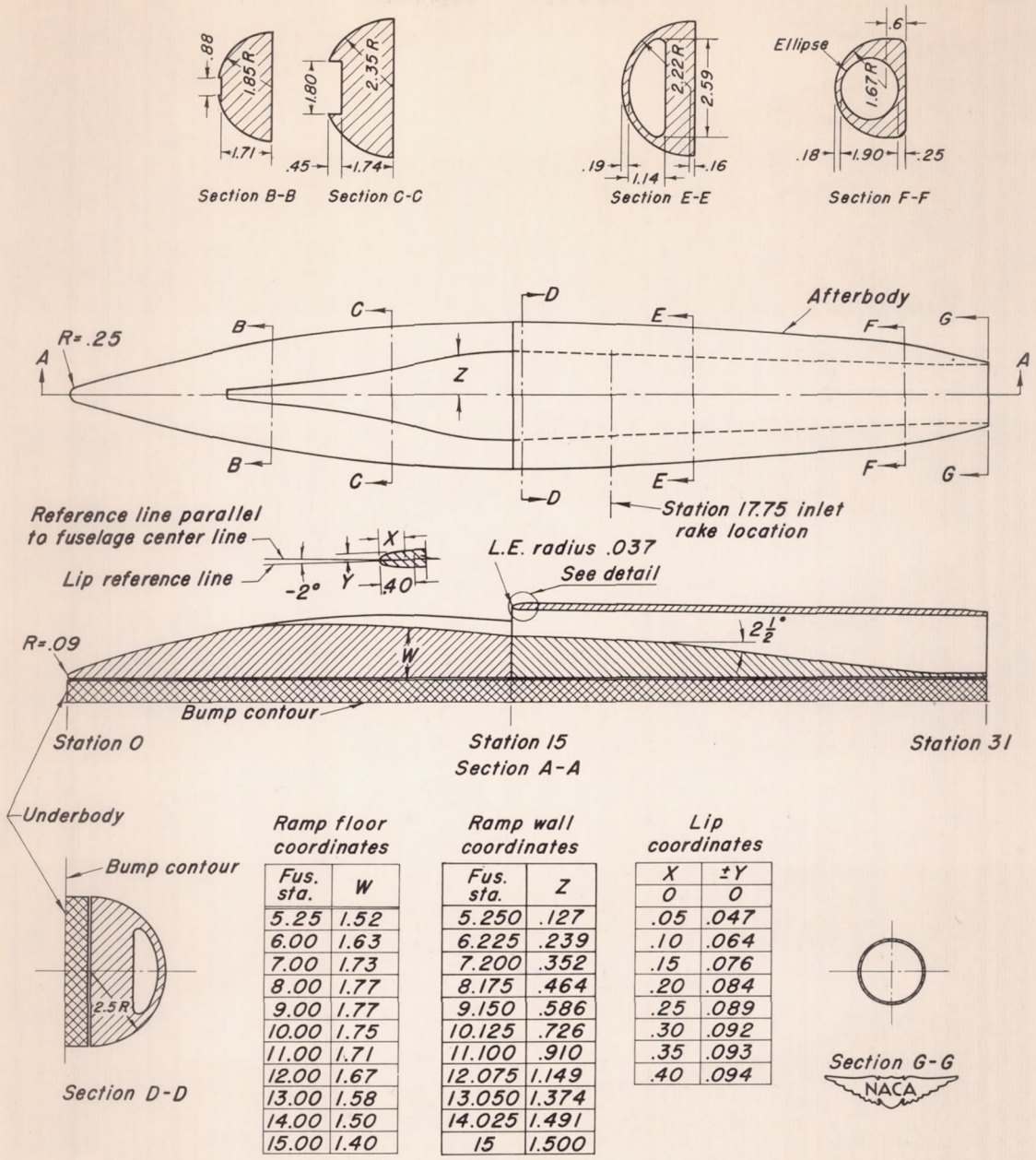

Ramp floor coordinates

Fus. sta.	W
5.25	1.52
6.00	1.63
7.00	1.73
8.00	1.77
9.00	1.77
10.00	1.75
11.00	1.71
12.00	1.67
13.00	1.58
14.00	1.50
15.00	1.40

Ramp wall coordinates

Fus. sta.	Z
5.250	.127
6.225	.239
7.200	.352
8.175	.464
9.150	.586
10.125	.726
11.100	.910
12.075	1.149
13.050	1.374
14.025	1.491
15	1.500

Lip coordinates

X	±Y
0	0
.05	.047
.10	.064
.15	.076
.20	.084
.25	.089
.30	.092
.35	.093
.40	.094

Note: All dimensions are in inches unless otherwise specified.

Figure 3.–Dimensions of afterbody and submerged inlet.

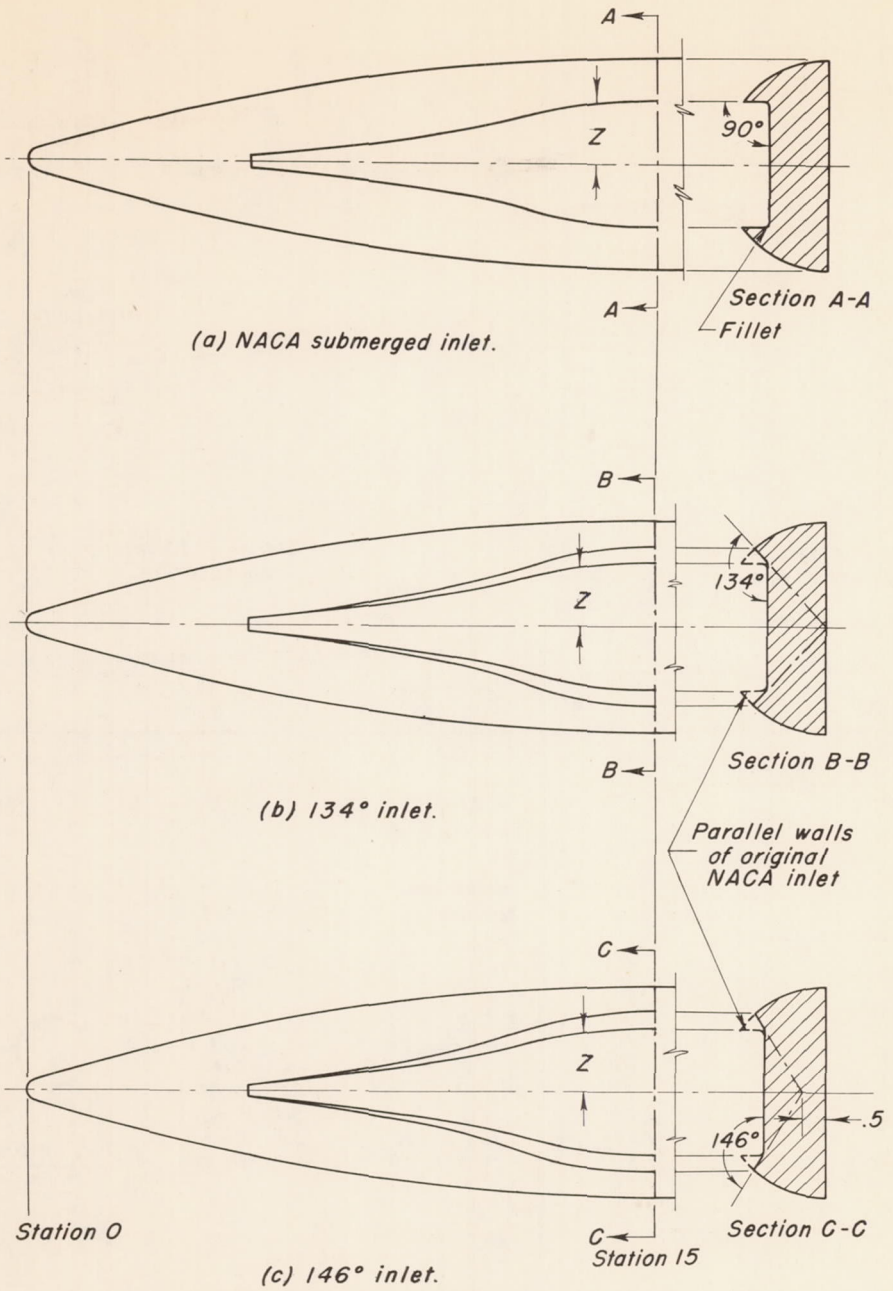

Note: The dimensions for Z are tabulated on figure 2. The NACA inlet was modified at each section as shown by the typical sections A-A and B-B. All dimensions are in inches.

Figure 4.—Dimensions of the three inlet models.

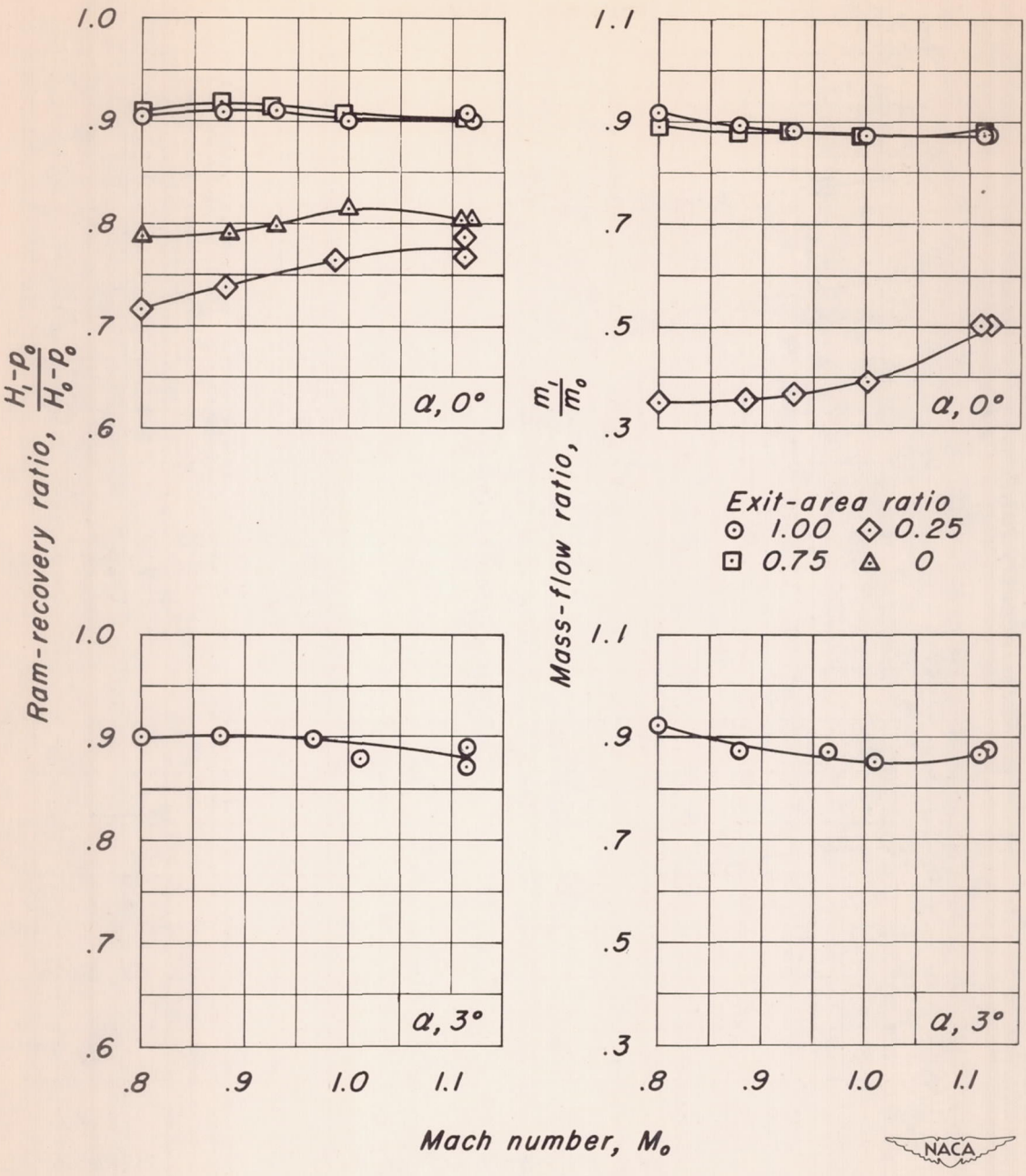

(a) Angle of attack, 0°, 3°.

Figure 5.–Variation of ram-recovery ratio and mass-flow ratio with Mach number at the inlet rake for the NACA submerged inlet.

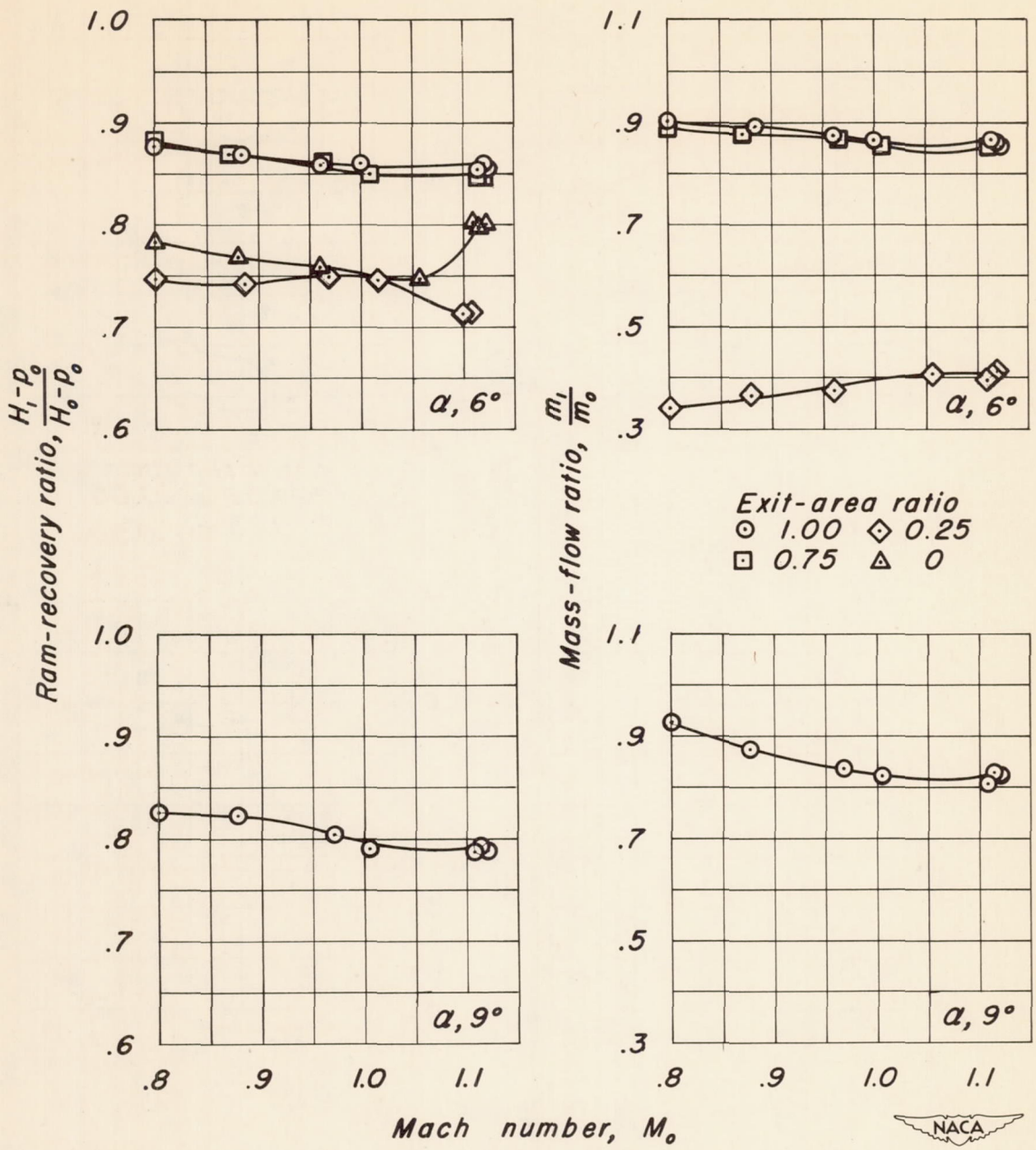

(b) Angle of attack, 6°; 9°

Figure 5.– Concluded.

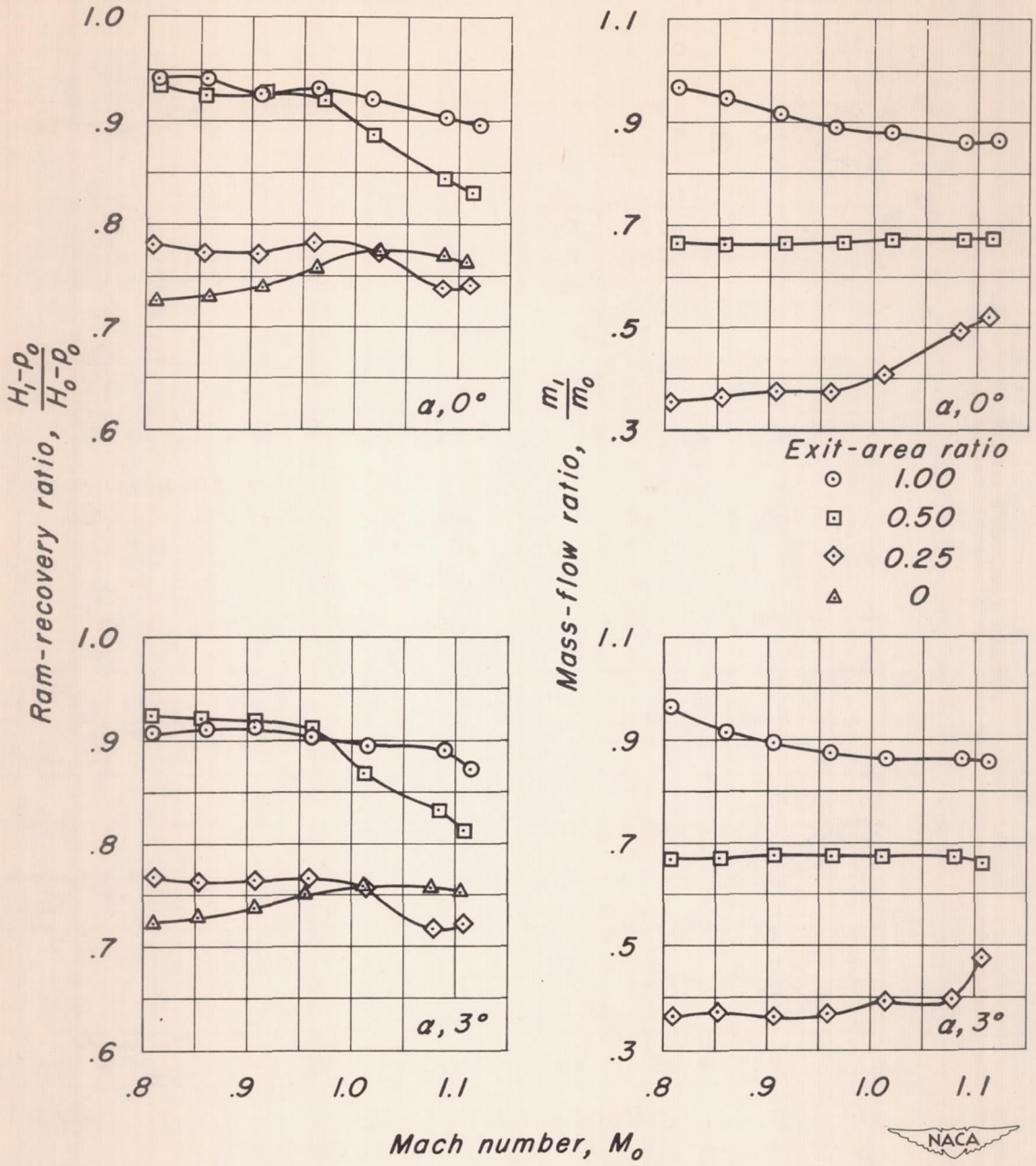

(a) Angle of attack, 0°, 3°

Figure 6.–Variation of ram-recovery ratio and mass-flow ratio with Mach number at the inlet rake for the 134° inlet.

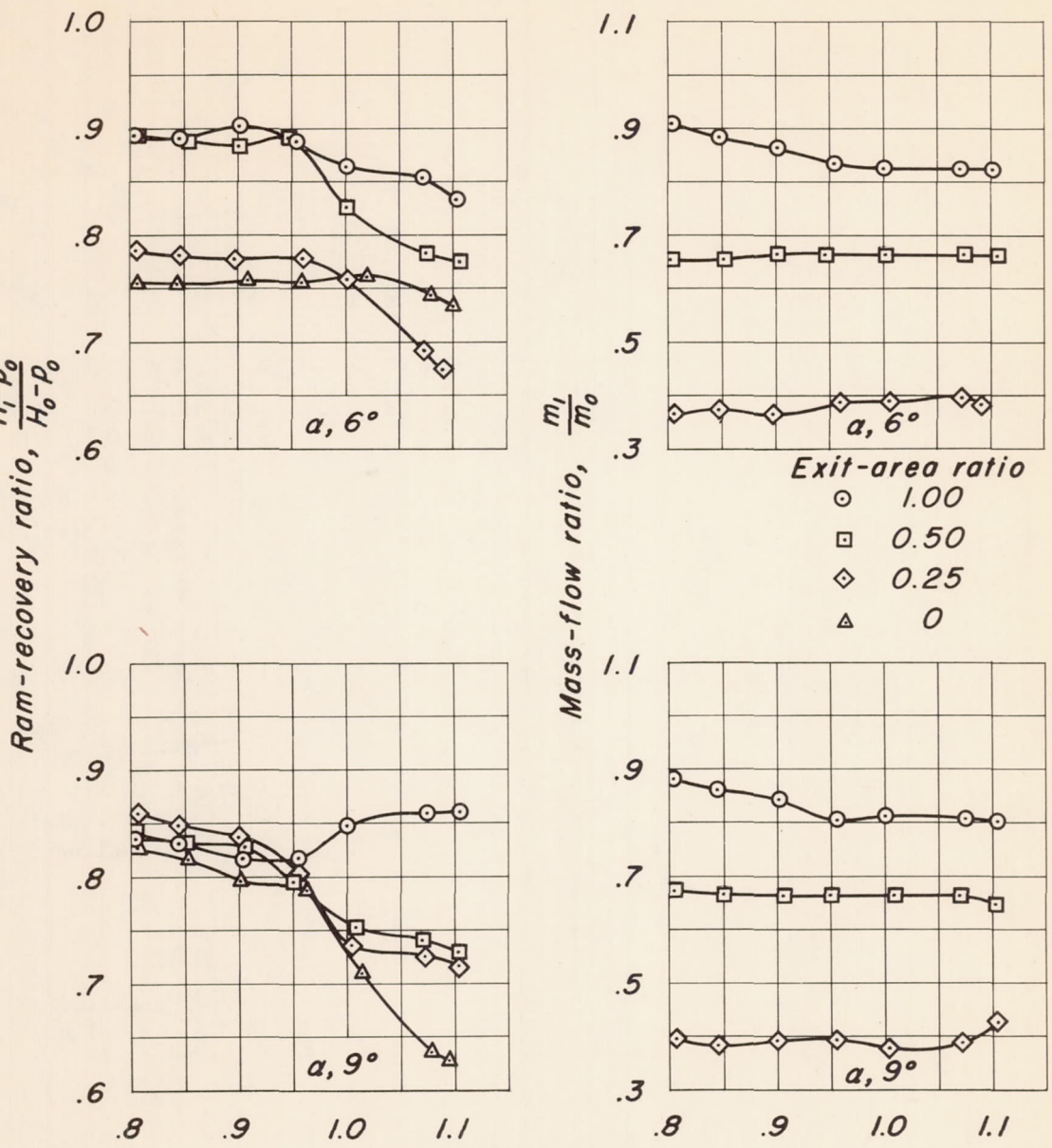

(b) Angle of attack, 6°, 9°.

Figure 6.—Concluded.

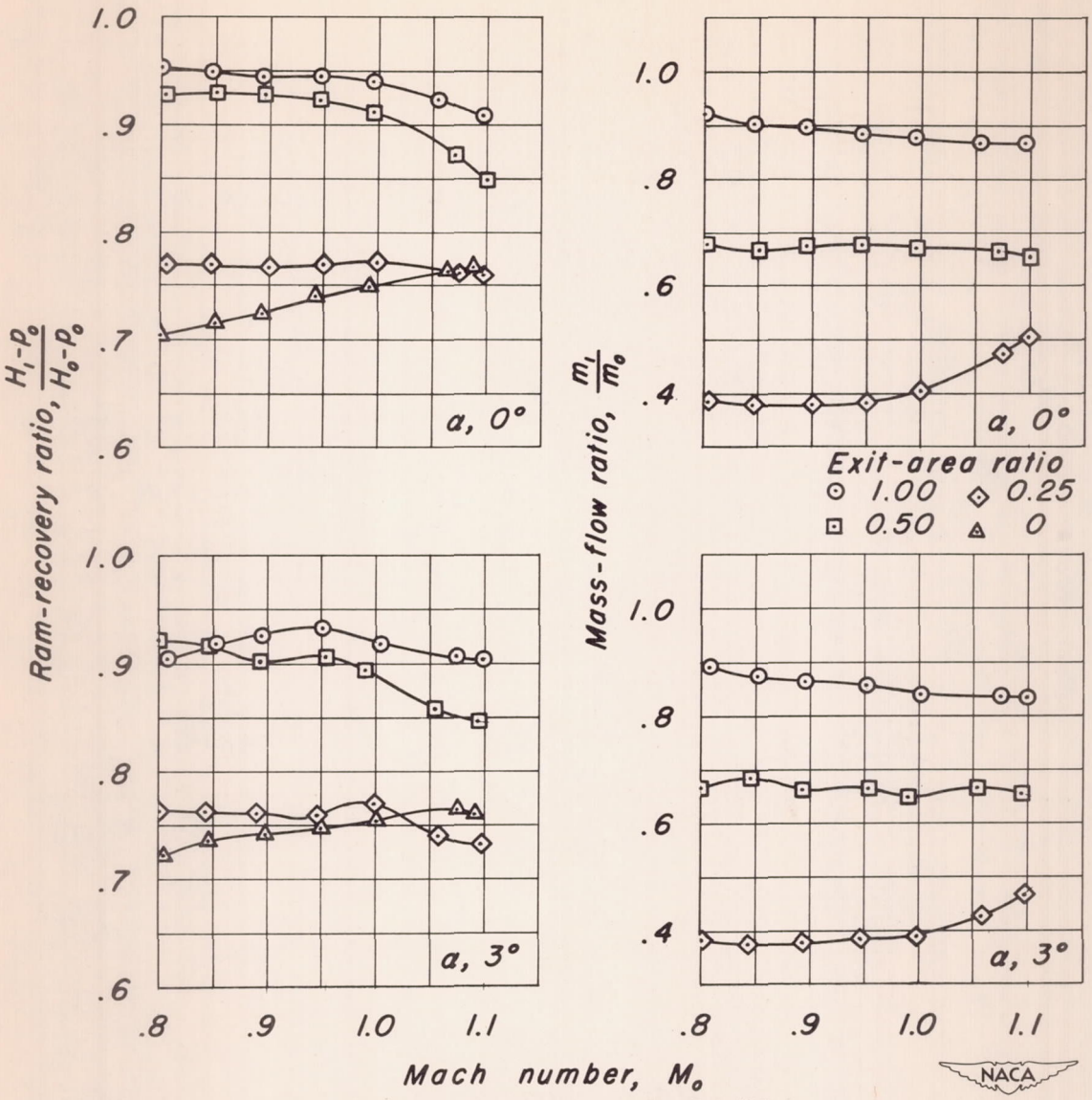

(a) Angle of attack, 0°, 3°.

Figure 7.- Variation of ram-recovery ratio and mass-flow ratio with Mach number at the inlet rake for the 146° inlet.

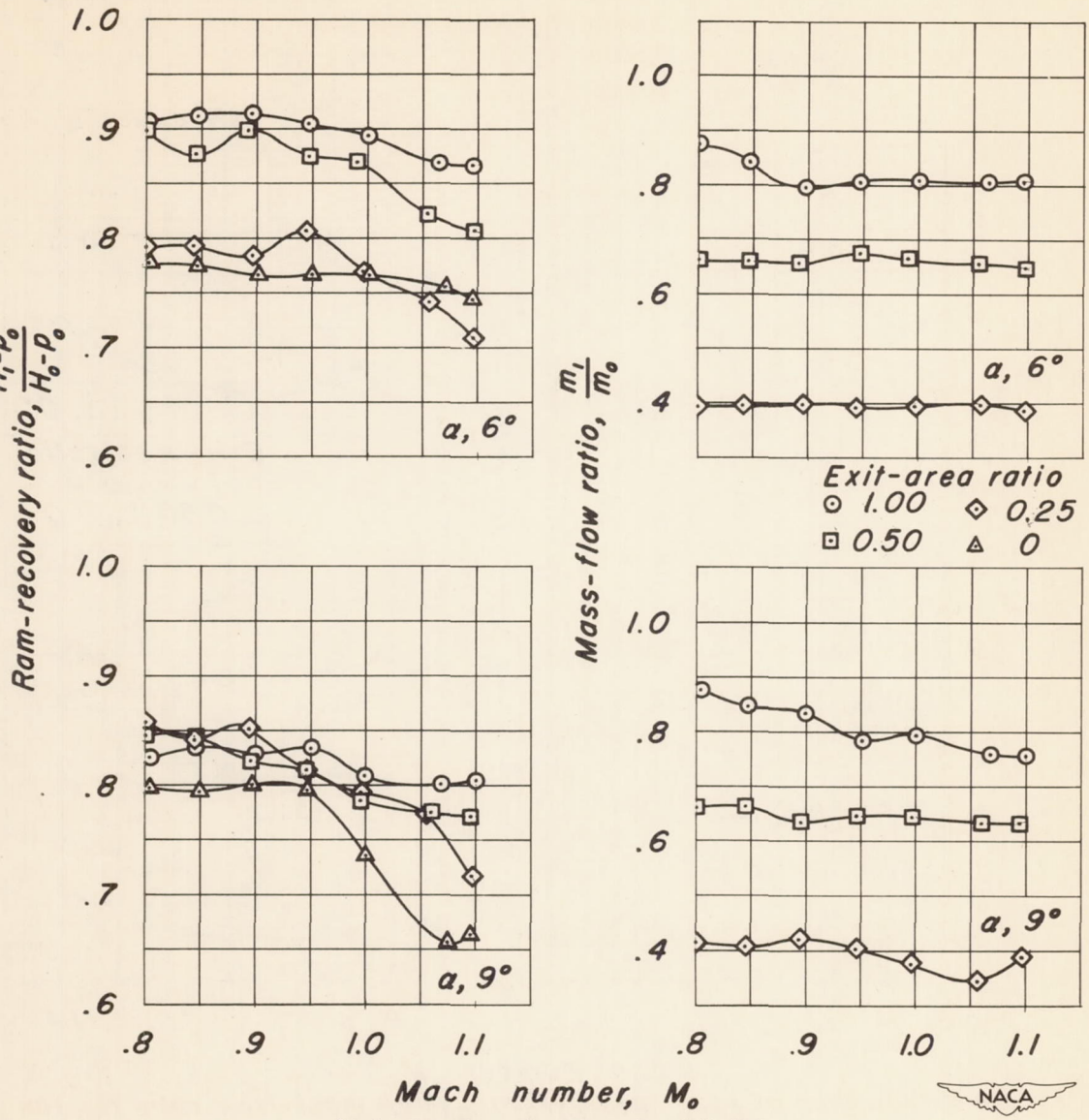

(b) Angle of attack, 6°, 9°

Figure 7.—Concluded.

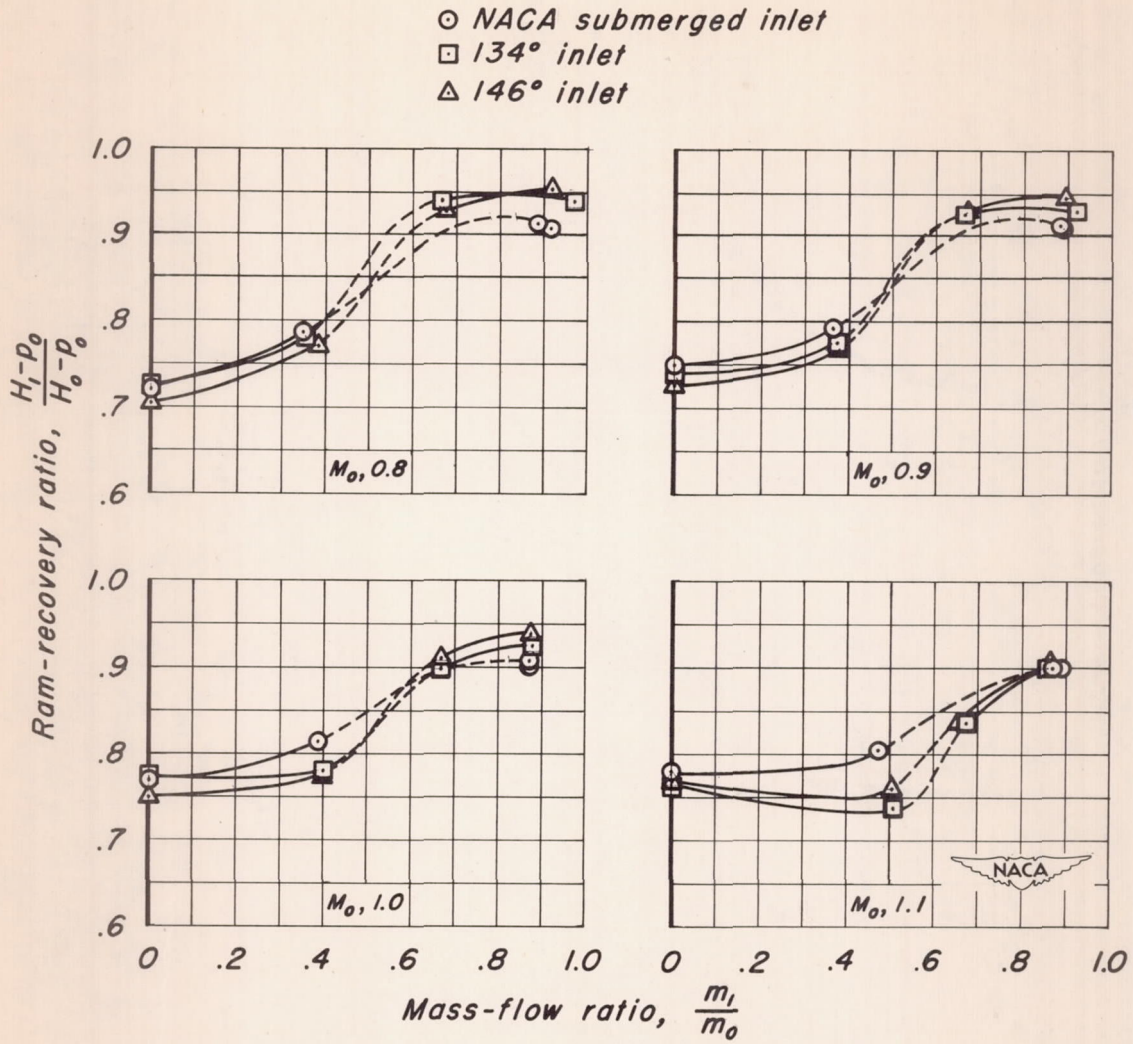

(a) Angle of attack, 0°.

Figure 8.–Variation of ram-recovery ratio with mass-flow ratio for the three inlets at four Mach numbers and four angles of attack.

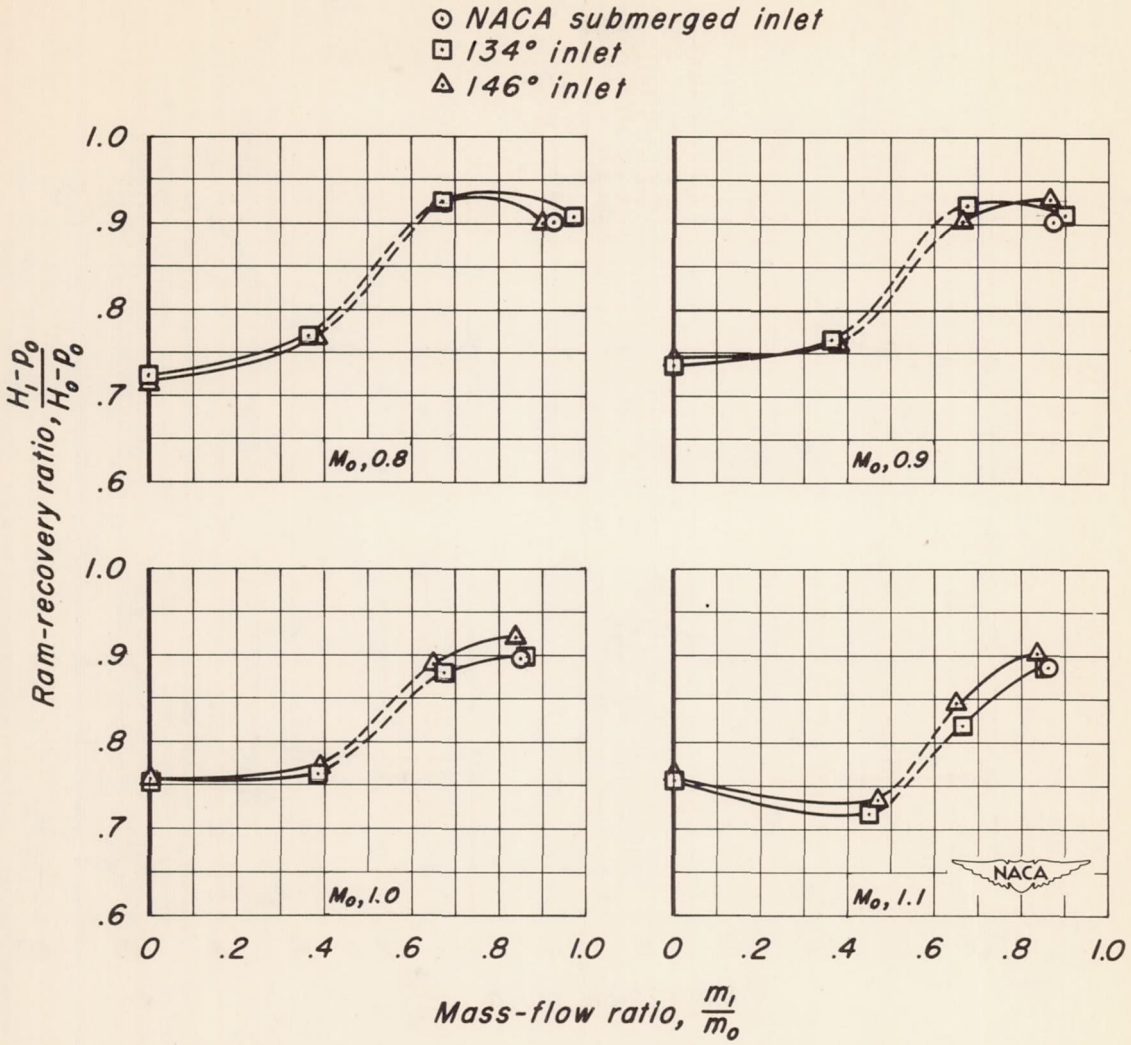

(b) Angle of attack, 3°

Figure 8.—Continued.

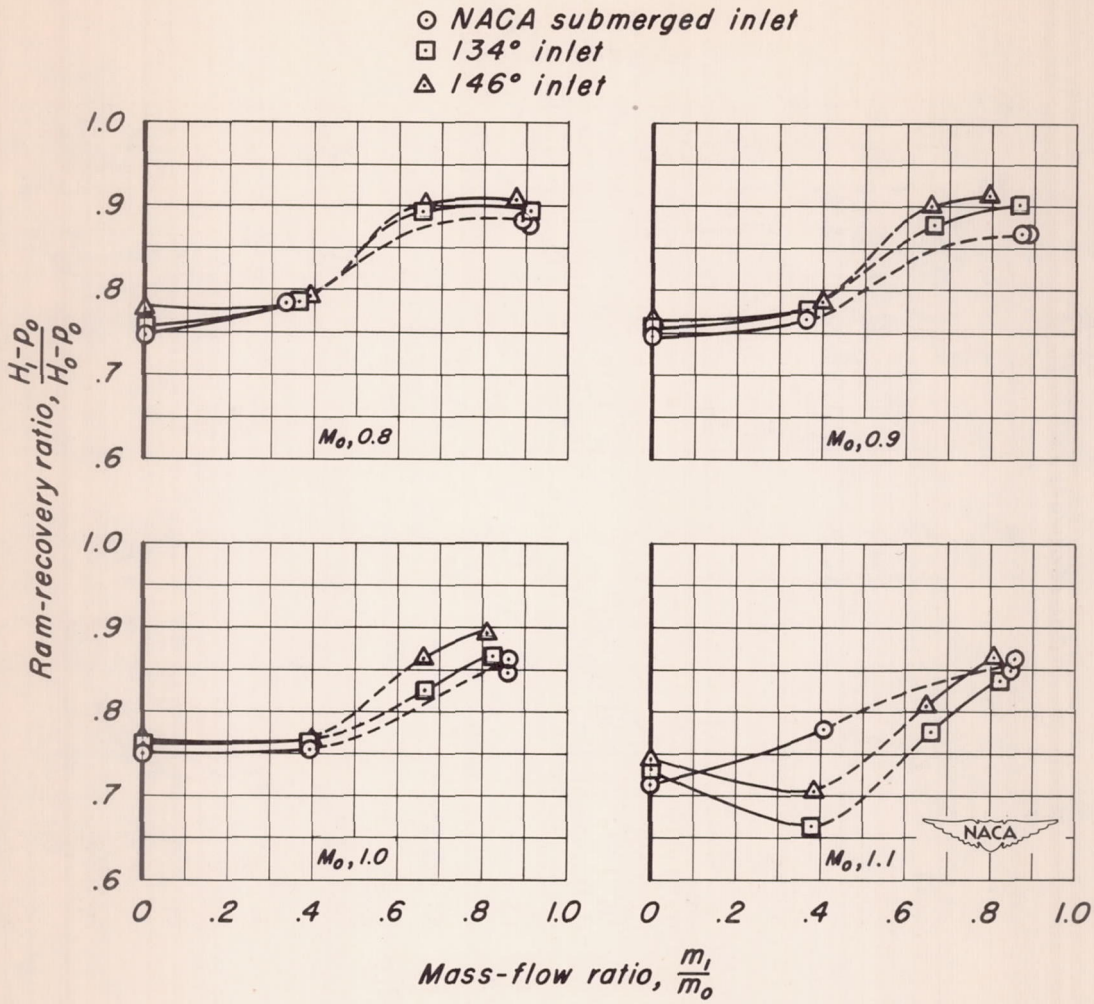

(c) Angle of attack, 6°

Figure 8.—Continued.

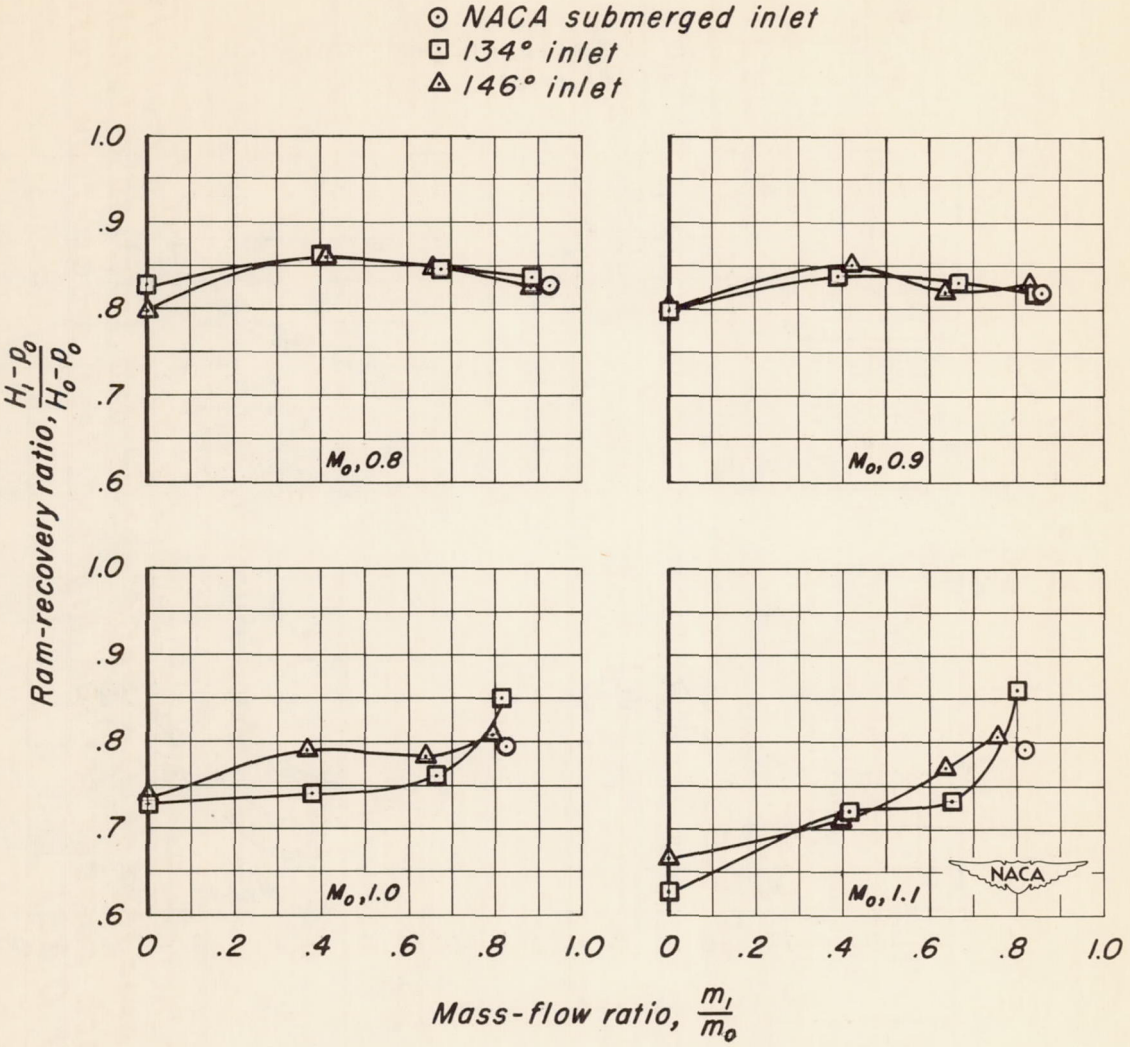

(d) Angle of attack, 9°

Figure 8.—Concluded.

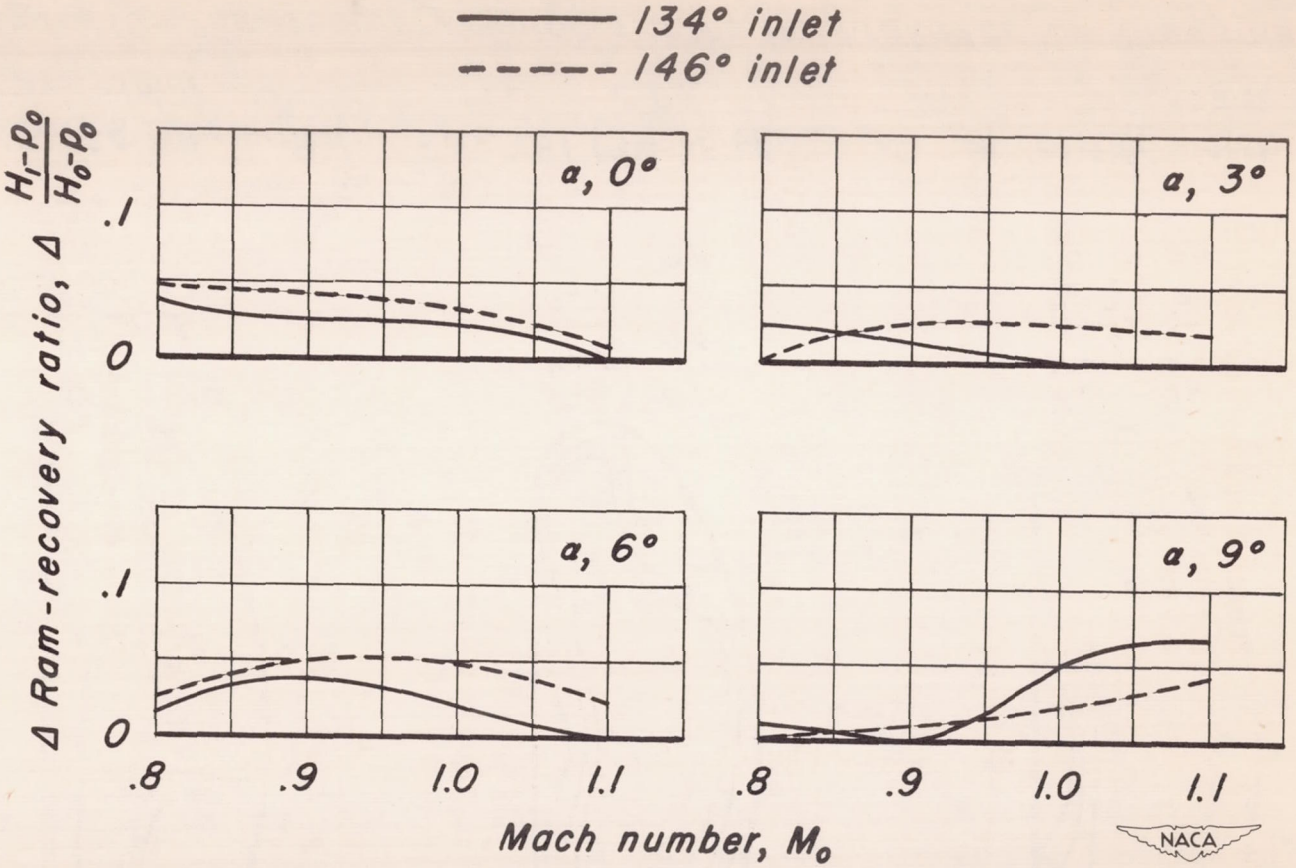

Figure 9.–Increment of ram-recovery ratio for the modified inlets over that of the NACA submerged inlet as a function of Mach number for the highest test mass-flow ratios (about 0.88).

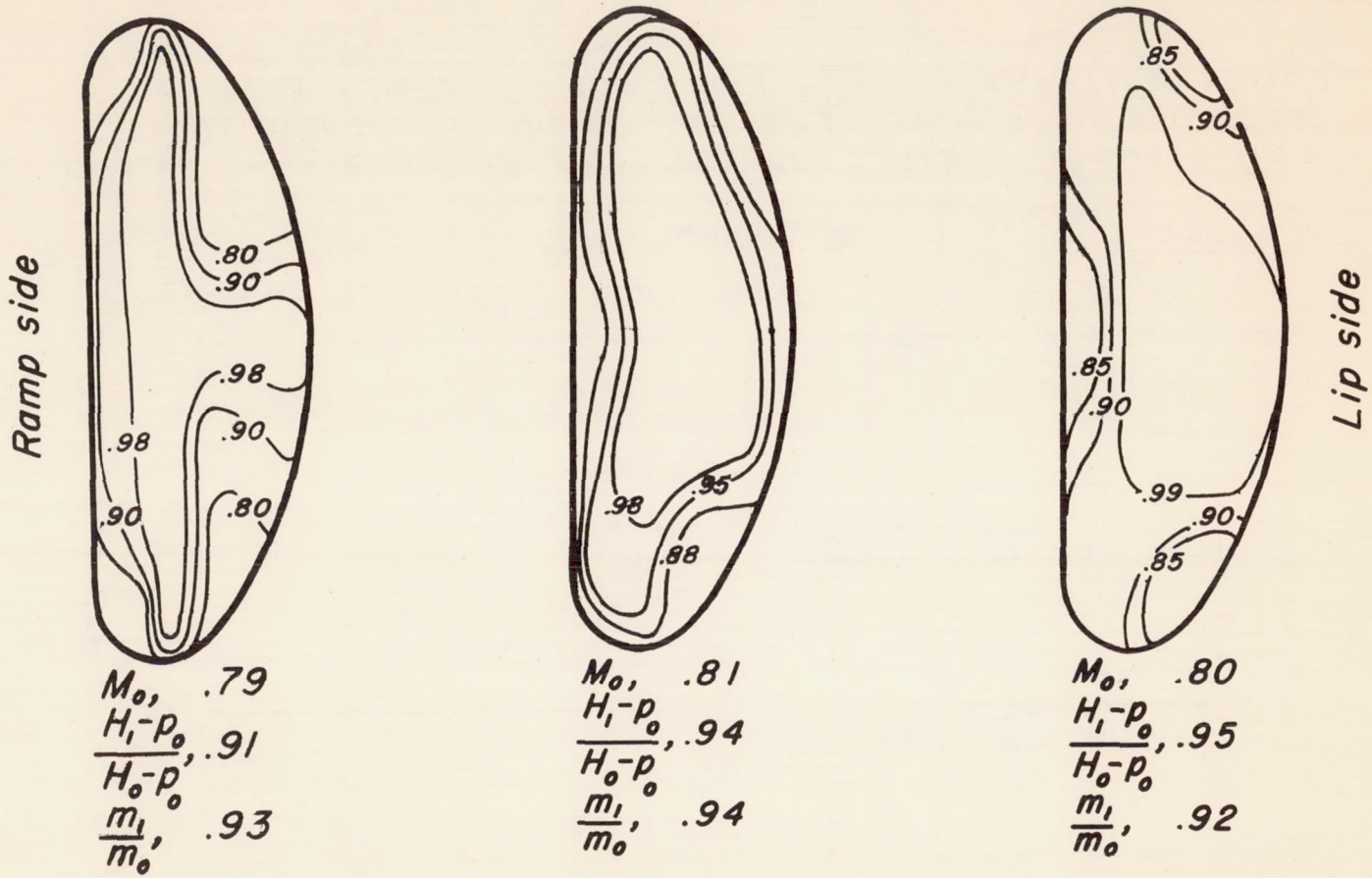

Figure 10.–Ram-recovery contours at the inlet rake for the three inlets for one Mach number. α, 0°.

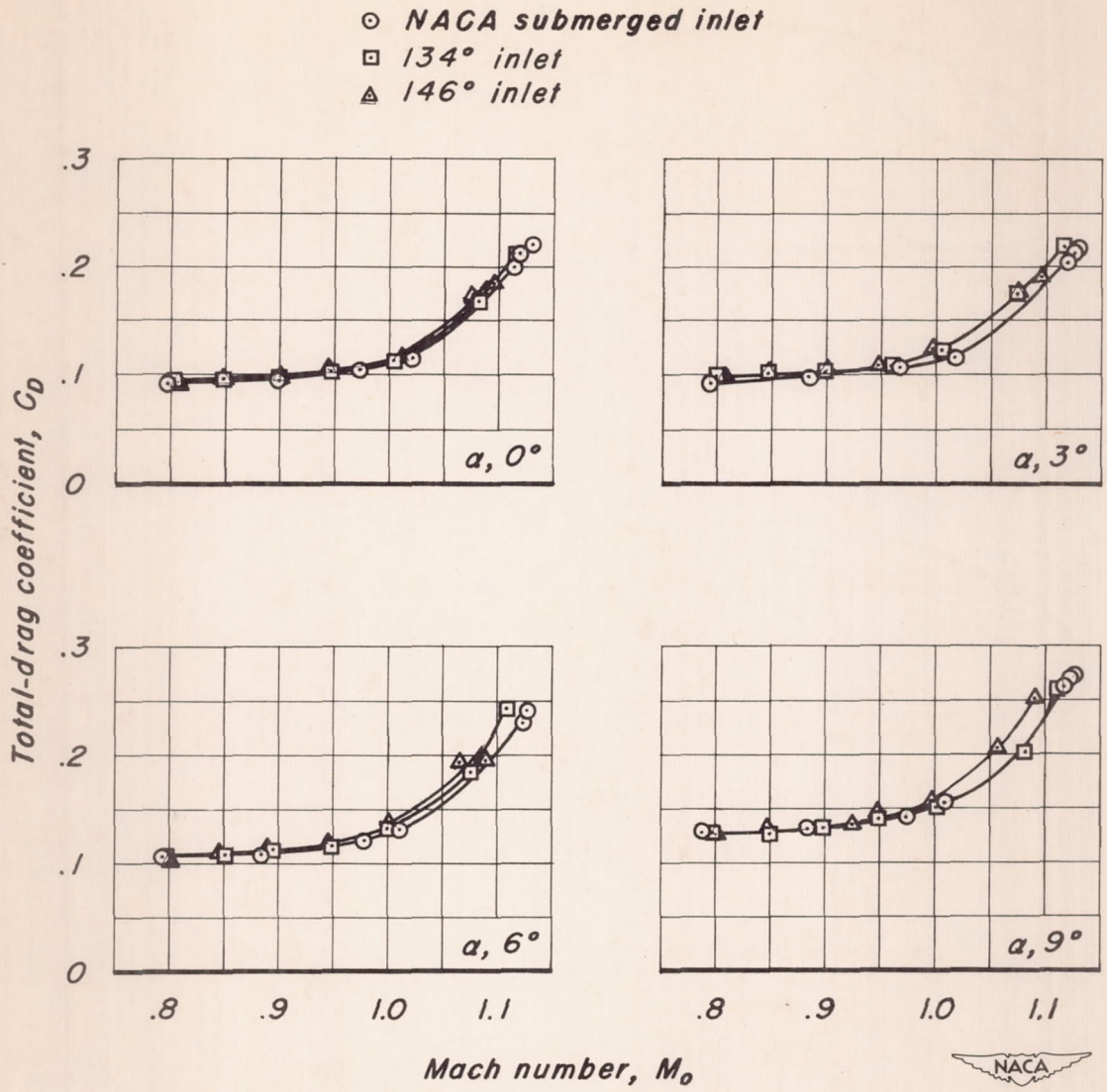

Figure 11.–Variation of total-drag coefficient with Mach number for the three inlets at four angles of attack. $\frac{m_1}{m_o} \approx 0.88$.